Nonlinear response of radiatively coupled intersubband transitions of quasi-two-dimensional electrons

T. Shih,[1,*] K. Reimann,[1,†] M. Woerner,[1,‡] T. Elsaesser,[1] I. Waldmüller,[2,§] A. Knorr,[2] R. Hey,[3] and K. H. Ploog[3]
[1]*Max-Born-Institut für Nichtlineare Optik und Kurzzeitspektroskopie, 12489 Berlin, Germany*
[2]*Institut für Theoretische Physik, Technische Universität Berlin, 10623 Berlin, Germany*
[3]*Paul-Drude-Institut für Festkörperelektronik, 10117 Berlin, Germany*
(Received 2 September 2005; published 23 November 2005)

Radiative coupling of resonantly excited intersubband transitions in GaAs/AlGaAs multiple quantum wells can have a strong impact on the coherent nonlinear optical response, as is shown by phase and amplitude resolved propagation studies of ultrashort electric field transients. Upon increasing the driving field amplitude, strong radiative coupling leads to a pronounced self-induced absorption, followed by a bleaching due to the onset of delayed Rabi oscillations. A many-particle theory including light propagation effects accounts fully for the experimental results.

DOI: 10.1103/PhysRevB.72.195338 PACS number(s): 78.67.De, 03.67.−a, 42.65.Re, 73.21.Fg

I. INTRODUCTION

Optical spectroscopy is one of the main sources of information about the properties of quantum systems. Obviously, for this to work it is necessary that the system under study couples to radiation. In most cases it is sufficient to consider this radiative coupling just as a tool that does not influence the properties of the system, especially not its dynamics. A consequence of weak radiative coupling is Beer's law, i.e., the absorption coefficient is proportional to the density of particles.

If the radiative coupling is strong, however, it can dominate the optical properties of the system via the reemitted fields. The strength of the radiative coupling depends on the density of those particles that can act together coherently, and on the coupling strength of each particle. The effect of radiative coupling is that the field acting on a system is modified by the system itself and by other systems, i.e., field sources, in the neighborhood, resulting in a radiative coupling within the ensemble of quantum systems.

Quasi-two-dimensional semiconductor quantum structures are important model systems for studying linear and nonlinear radiative coupling effects.[1–5] In high-quality quantum well samples, excitons in photonic Bragg and anti-Bragg structures or microcavities can experience significant radiative coupling. For a study of the effects of radiative coupling excitons have, however, the disadvantage that the coupling strength is mainly determined by the material properties and thus very difficult to vary significantly without changing other properties of the system (e.g., exciton binding energy and dephasing rate). In contrast, the coupling strength of intersubband (IS) transitions[6] in *n*-type modulation-doped MQWs can be varied quite easily in a broad range by changing the carrier density in otherwise identical structures.

So far, there are only few theoretical studies considering the influence of radiative coupling effects on the linear response of coherent IS transitions in MQWs.[7–11] Except for the work reported in Ref. 12, a systematic experimental study of radiative coupling effects in linear IS absorption is still missing. The role of radiative coupling for the nonlinear response of IS transitions in MQWs has remained totally unexplored.

In this paper, we demonstrate for the first time the impact of radiative coupling on the nonlinear response of IS transitions in MQWs. Coherent nonlinear propagation experiments on two structurally identical GaAs/AlGaAs quantum well samples with different radiative coupling reveal an entirely different optical response. Upon increasing the amplitude of the excitation we find for weak radiative coupling the expected decrease,[13] for strong radiative coupling, however, a pronounced increase of the IS absorption. This phenomenon is caused by the strong modification of the local fields acting on the QWs by the reemitted fields, leading to a coupling of all QWs through transverse electromagnetic fields. A many-particle theory including light propagation effects is in good agreement with the experiments and provides deeper insights into the detailed dynamics of the entire quantum structure.

We begin with the description of the samples used in our experiments (Sec. II). An important point here is the geometry of light propagation. Then we show results of linear IS absorption measurements, followed by an explanation in a very simple model (Sec. III). Next we present the results of our nonlinear transmission experiments (Sec. IV). The explanations for these results are given in Secs. V and VI. After the conclusions (Sec. VII) follows an Appendix with the detailed equations used in the microscopic theory.

II. SAMPLES

We investigated two *n*-type modulation-doped MQW samples consisting each of 51 electronically uncoupled GaAs QWs of 10 nm width, separated by 20 nm thick $Al_{0.35}Ga_{0.65}As$ barriers, the centers of which are δ-doped with Si [Fig. 1(a)]. Sample *L* has a low electron density of $n_s = 5 \times 10^{10}$ cm^{-2} per QW and sample *H* a high density of $n_s = 1.2 \times 10^{12}$ cm^{-2}. The samples were processed into prisms [Fig. 1(b)] to achieve a strong coupling of the *p*-polarized MIR pulse and the IS transition dipoles. The incident field $E_{in}(t)$ enters through the side facet, travels through the whole stack of QWs and is totally reflected from the bottom surface

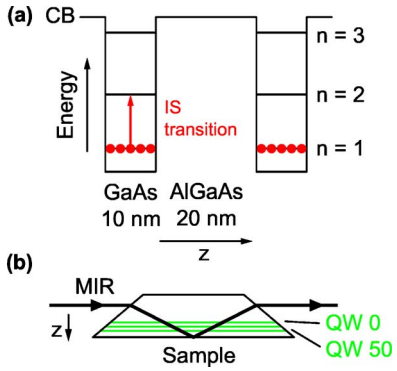

FIG. 1. (Color online) (a) Schematic of the *n*-type modulation-doped GaAs/AlGaAs multiple quantum well sample containing 51 GaAs quantum wells. (b) Light propagation within our prism-shaped multiple quantum well sample.

of the prism. The reflected wave interacts a second time with the stack of QWs and $E_{\text{out}}(t)$ leaves the sample through the other side facet. The thickness of the layer between the QWs and the prism base is chosen so that the wave reflected at the prism base is again in phase (phase shift of 2π, consisting of the phase shift caused by the optical path length and of the phase shift upon total reflection) with the incident wave in the center of the QW stack. In an undoped sample, i.e., one without IS absorption, this geometry leads to a standing wave pattern perpendicular to the layers having its antinode at the center of the QW stack (for details see Refs. 11 and 14). Besides the strong coupling of the MIR pulse to the IS transition dipoles this geometry was chosen because it has only one output for the light, which greatly facilitates the measurement of the absorption in the sample. In this geometry the optical power absorbed by the QWs is simply proportional to $\int E_{\text{in}}(t)^2 dt - \int E_{\text{out}}(t)^2 dt$.[15]

III. LINEAR INTERSUBBAND ABSORPTION

The linear IS absorption spectra of the two samples at different lattice temperatures T_L are presented in Fig. 2. Both samples show narrow absorption lines of comparable width for the $1 \leftrightarrow 2$ IS transition around 100 meV. Surprisingly, the $1 \leftrightarrow 2$ absorption strength of sample *H* [Fig. 2(b)] is comparable to that of sample *L* [Fig. 2(a)], although the electron density of sample *H* is 24 times higher—a clear violation of Beer's law caused by strong radiative coupling. Sample *H* shows an additional absorption band around $\hbar\omega = 120$ meV for higher lattice temperatures, due to IS transitions of thermally excited electrons in the $n=2$ subband (at $T_L = 300$ K 1.8% and at $T_L = 250$ K 0.8% of the $n=1$ electrons) into the $n=3$ subband. In contrast to the $1 \leftrightarrow 2$ absorption band the absorption strength of the $2 \leftrightarrow 3$ band obeys Beer's law as a function of the population in the $n=2$ subband.

How radiative coupling leads to the surprising absorption results can be explained in a simple model, which follows the lines of Ref. 16. In our case it is a very good approximation to consider the radiation as plane waves.[17] Further, our experimental geometry, i.e., *p*-polarized waves under an angle of incidence of 60° [Fig. 1(b)], can be converted into a

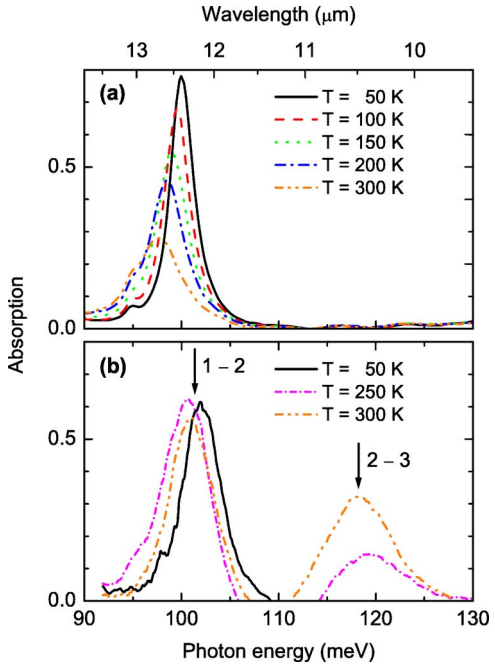

FIG. 2. (Color online) Measured linear IS absorption spectra of two structurally identical multiple quantum well samples with different electron densities per quantum well n_s for various lattice temperatures. (a) Sample *L* with $n_s = 5 \times 10^{10}$ cm^{-2}. (b) Sample *H* with $n_s = 1.2 \times 10^{12}$ cm^{-2}. At higher lattice temperatures one observes for *H* additionally the $2 \leftrightarrow 3$ IS transition of thermally excited electrons in the $n=2$ subband.

one-dimensional propagation scheme (similar to Fig. 1 of Ref. 16).

Before considering the geometry of the actual experiment, we will begin by considering a single QW interacting with a monochromatic, electromagnetic wave E_{in} [Fig. 3(a)]. The derivation of the equations discussed in the following and more details can be found in Ref. 16. The local field E_{lo} at the QW creates a macroscopic IS polarization in the QW, which in turn emits two electromagnetic waves with equal amplitudes E_{em} into the forward and into the backward (reflected, $E_{\text{re}} = E_{\text{em}}$) direction. In the forward direction E_{in} and E_{em} interfere, leading to the transmitted wave $E_{\text{tr}} = E_{\text{in}} + E_{\text{em}}$. The interference between E_{in} and E_{em} leads to a modification of the local field E_{lo}, which is not equal to the incident field but equal to the transmitted field $E_{\text{lo}} = E_{\text{tr}}$. Exactly this modification is the cause of the radiative coupling phenomena dealt with in this paper.

In the linear regime, i.e., for low amplitudes of E_{in}, and in resonance, the emitted field E_{em} is out of phase with E_{lo}, i.e., $E_{\text{em}} = -\xi E_{\text{lo}}$, resulting in the expected attenuation of the transmitted wave. The dimensionless radiative coupling parameter ξ is proportional to the sheet carrier density n_s and to the IS absorption cross section σ_{IS} (σ_{IS} is proportional to the square of the transition dipole matrix element and inversely proportional to the linewidth): $\xi = \frac{1}{2} n_s \sigma_{\text{IS}}$. Solving for E_{em} and E_{lo}, we get the results shown in Fig. 3(c) as a function of ξ for the transmission $T = (E_{\text{tr}}/E_{\text{in}})^2 = 1/(1+\xi)^2$, the reflection $R = (E_{\text{re}}/E_{\text{in}})^2 = [\xi/(1+\xi)]^2$, and the absorption $A = 1 - R - T = 2\xi/(1+\xi)^2$. For comparison we also show the absorption

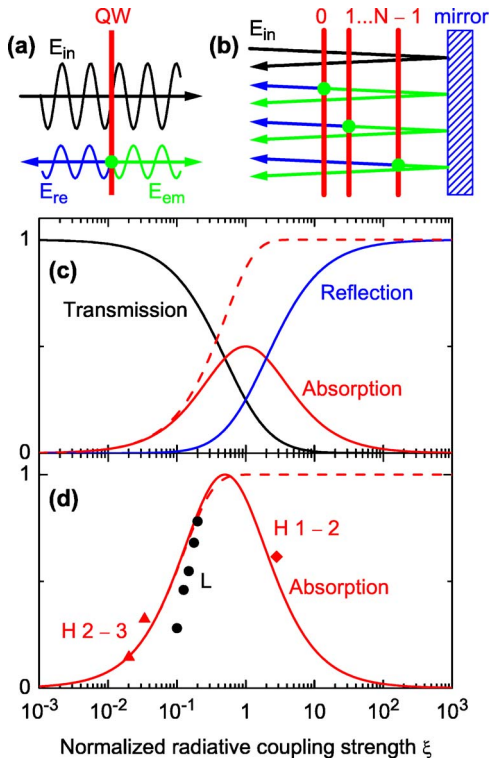

FIG. 3. (Color online) (a) Linear IS absorption of a single QW corresponds to the destructive interference of the incident wave E_{in} with the wave E_{em} coherently emitted by the macroscopic IS polarization resulting in an attenuated transmitted wave E_{tr}. The QW also emits a reflected wave $E_{re}=E_{em}$. (b) Schematic of the relevant interacting waves in our multiple QW samples showing additionally total reflection of all waves at the base of the prism. (c) Solid lines, transmission, reflection, and absorption of light resonant to the IS transition of a single QW as a function of the radiative coupling parameter ξ. (d) Solid line, calculated absorption for situation (b) together with experimental values (symbols) obtained from temperature-dependent linear IS absorption spectra (Fig. 2) (Ref. 18). The dashed lines in (c) and (d) are values according to Beer's law.

according to Beer's law (dashed line), $A_{Beer}=1-\exp(-2\xi)=1-\exp(-n_s\sigma_{IS})$. In this approximation, which is valid for weak radiative coupling, i.e., for $\xi \ll 1$, absorption does not lead to a reflected wave and the local field is equal to the incident field. Starting around $\xi \approx 0.2$, the inclusion of radiative coupling leads to significantly different results. Contrary to Beer's law, which shows a monotonic increase of the absorption with ξ, radiative coupling results in an absorption maximum of $A=0.5$ at $\xi=1$ and in $A \to 0$ for $\xi \to \infty$. In the latter case, the incident field is fully reflected from the QW.

Unfortunately, values of $\xi > 0.2$ are hardly achievable for IS transitions in a single QW. However, several QWs can emit in phase and thus act together if their distances are small compared to the wavelength of the transition. For simplicity we will assume here perfect constructive interference of all waves involved, which corresponds to the hypothetical situation that all QWs are at the same spatial position.[19] ξ has then N times (N is the number of QWs) the value of a single QW. The low-temperature values of ξ for the $1 \leftrightarrow 2$ IS transition for our two samples are $\xi_L=0.2$ and $\xi_H=3$, showing that sample L is in the regime of weak radiative coupling and sample H in the regime of strong radiative coupling.

A further increase of the effect of radiative coupling is achieved by using the light propagation geometry shown in Fig. 1(b). Here the local field E_{lo} experienced by the individual QWs is the sum of the incident wave E_{in} and the reemitted waves of all QWs plus all totally reflected waves at the base of the prism [mirror in the schematic in Fig. 3(b)].[13,16,20]

In this geometry the local field is $E_{lo}=2E_{in}/(1+2\xi)$ and the absorption $A=8\xi/(1+2\xi)^2$ [see solid line in Fig. 3(d)]. For weak radiative coupling ($\xi \ll 1$) the local field has double the amplitude of the incident field because of the standing wave formed at the mirror. For larger ξ the local field decreases and becomes even smaller than the incident field for $\xi > 0.5$. The absorption as a function of ξ is quite similar to that of a single QW shown in Fig. 3(c). The main differences are that the maximum absorption is now $A=1$ and that it occurs at $\xi=0.5$. Again the dashed line shows the absorption using Beer's approximation, which now reads $A_{Beer}=1-\exp(-8\xi)=1-\exp(-4Nn_s\sigma_{IS})$.

The symbols in Fig. 3(d) show for comparison the experimental values[18] obtained from the measured linear IS absorption spectra (Fig. 2). We observe quite good agreement with the simple model discussed above, which shows that the surprisingly weak IS absorption of sample H is a direct consequence of the strong radiative coupling in this sample.

IV. NONLINEAR TIME-RESOLVED EXPERIMENTS

The nonlinear optical properties of both samples are investigated in coherent propagation experiments.[13] 200 fs midinfrared pulses with a center frequency resonant to the $1 \leftrightarrow 2$ IS transition, generated by optical rectification of intense 25 fs pulses at 800 nm in a thin GaSe crystal,[21] interact with the sample in the propagation geometry shown in Fig. 1(b). The electric field of the incident light $E_{in}(t)$ and the electric field of the light transmitted through the sample $E_{out}(t)$ are fully characterized by ultrafast electro-optic sampling.[22] Experiments at a temperature of 100 K were performed for different field strengths of the excitation pulses.

Figure 4 shows electric field transients $E_{out}(t)$ transmitted through sample H for different amplitudes of the input field. The corresponding results[23] for sample L are given in Ref. 13. The electric field measured by electro-optic sampling is plotted as a function of time (solid line). The dashed lines represent the electric field envelope of the input pulse. The temporal position of the input envelope was determined by transmitting pulses through an undoped reference sample with negligible IS absorption. The field amplitude in Fig. 4(a) of 5 kV/cm is low enough to show a linear response, namely a slightly lower amplitude of $E_{out}(t)$ compared to $E_{in}(t)$ during the pulse and a damped oscillation afterwards (free-induction decay). For intermediate amplitudes one gets complex output transients [Fig. 4(b)], which show a surprisingly low amplitude compared to $E_{in}(t)$. For very high amplitudes [Fig. 4(c)] the transmitted field $E_{out}(t)$ gradually ap-

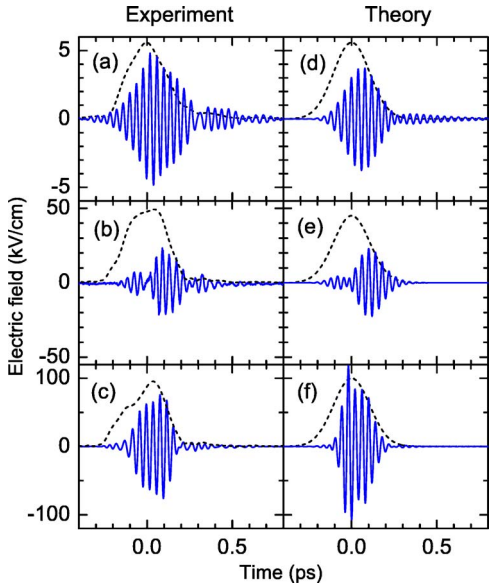

FIG. 4. (Color online) (a)-(c) Electric field transients measured after sample H (electron density of $n=1.2\times10^{12}$ cm^{-2} per QW) for incident field amplitudes of (a) 5 kV/cm, (b) 45 kV/cm, and (c) 100 kV/cm. Dashed line, field envelopes of the input pulses. (d)–(f) Both the shape and the amplitude of the theoretically calculated transients are in good agreement with the corresponding experimental counterparts (a)–(c).

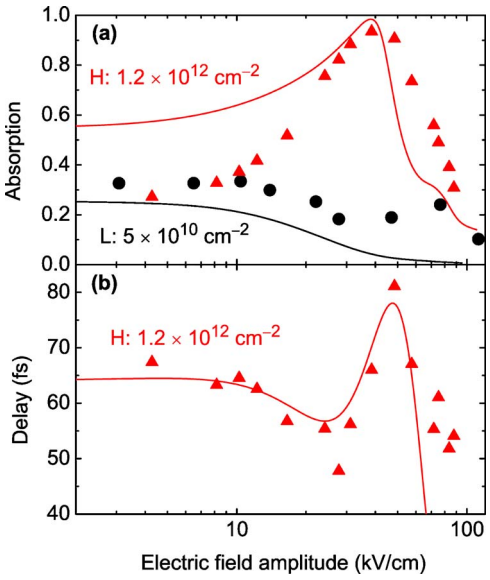

FIG. 5. (Color online) (a) Absorption of a femtosecond infrared pulse resonant to the IS transition in sample H (triangles) and in sample L (dots) as a function of the incident pulse amplitude. (b) Delay of the center of gravity of the pulse transmitted through sample H. Solid lines, many-body calculations with excitation-induced dephasing.

proaches the shape and amplitude of the corresponding $E_{\text{in}}(t)$. Figures 4(d)–4(f) show the corresponding results of the microscopic theory, which is the subject of Sec. VI.

From such measurements, we derive both the absorption of the two samples, given by[15]

$$A = 1 - \int E_{\text{out}}(t)^2 dt \Big/ \int E_{\text{in}}(t)^2 dt, \tag{1}$$

and the delay of the center of gravity of the pulse $\int tE(t)^2dt/\int E(t)^2dt$ compared to a pulse transmitted through an undoped reference sample. In Fig. 5, these quantities are plotted as a function of the maximum amplitude of the incident electric field. For sample L [circles in Fig. 5(a)], one finds a decrease of the absorption (bleaching) with increasing amplitude according to the coherent driving of Rabi oscillations.[13] In contrast, the absorption of sample H (triangles) first increases with increasing pulse amplitude (induced absorption), reaches a maximum, and then decreases again. The pulse delay for sample H [Fig. 5(b)] first decreases slightly with increasing amplitude, reaches a maximum at about the same amplitude as the absorption maximum, and decreases again.

V. QUALITATIVE DISCUSSION

We now consider the influence of radiative coupling on the nonlinear optical response. As already discussed above [see Fig. 3(b)], the local electric field acting on an individual QW is determined by the incident field plus the fields reemitted from all QWs.[13,16,20] The reemitted fields in sample L are always small compared to the incident fields, whereas in sample H incident and reemitted fields are of similar magnitude in the linear regime. Strong reemitted fields lead to small local fields and thus to the comparably small linear $1\leftrightarrow2$ IS absorption observed for sample H [see Fig. 2(b)].

It is important to note that in the transient regime (in particular in the case when the driving pulse is shorter than the IS dephasing time) the constant relation between the reemitted field and the local field $E_{\text{em}}=-\xi\, E_{\text{lo}}$ does not hold anymore and must be replaced by a full time-dependent microscopic theory (see Sec. VI). The reason for this is that the emitted field $E_{\text{em}}(t)$ depends on the complete time-dependent history of the microscopic polarizations and populations created by E_{lo} in the past.

One advantage of the stationary model for linear absorption [Fig. 3(d)] presented in Sec. III is that its extrapolation to the stationary nonlinear case is straightforward. Thus, although we performed the nonlinear experiments with short pulses, it is instructive to consider the case of monochromatic resonant incident electric fields in the nonlinear regime. In this case the effect of radiative coupling on the nonlinear optical response can be explained easily with the help of Fig. 3(d). High incident fields lead to two well-known nonlinear effects: (i) population saturation of the IS transition and (ii) excitation induced dephasing.[24] Both phenomena result in a significant reduction of the radiative coupling parameter ξ. For low incident field amplitudes sample H starts at $\xi=3$ leading to the surprisingly low absorption. With increasing amplitude of E_{in} the value of ξ will be reduced thereby increasing the absorption up to its maximum at $\xi=0.5$. A further decrease of ξ results in a decrease of absorption and a corresponding increase in the amplitude of E_{out}. In contrast, sample L has a value of $\xi=0.2$ in the linear regime. In this case any decrease in ξ only results in a decrease of absorption.

We are aware that this simple model cannot explain the detailed time dependence of the transmitted pulses. It is interesting, however, that it still gives for both samples a qualitative explanation for the dependence of absorption as a function of field amplitude observed in the time-resolved experiments [Fig. 5(a)]. The reason for this is that absorption is a time-integrated quantity [see Eq. (1)], so that any temporal variations of ξ are averaged out. The shape of the transmitted pulses and a quantitative calculation of the absorption as a function of electric-field amplitude can be provided by a full microscopic theory, which is the subject of the next section.

The center of gravity of the transmitted electric field transient is influenced by the free-induction decay of the IS polarization. With increasing incident field, the relative weight of the free induction decay becomes less and less, leading to a minimum in the pulse delay around 25 kV/cm. For even higher fields we reach effective pulse areas of π and higher. This results in a strong absorption of the first part of the pulse (most electrons are in the $n=1$ subband) and to weak absorption and even gain towards the end of the driving pulse (most electrons are in the $n=2$ subband). Thus, the center of gravity moves to longer delays. For high amplitudes the difference between the transmitted and the incident pulse becomes negligible and the delay should approach zero. Though this trend is evident from the data in Fig. 5, zero delay is not observed, probably because of nonlinear effects (increase of the refractive index for high intensities) in the GaAs substrate.

VI. MICROSCOPIC THEORY

To get deeper and quantitative insights into the detailed dynamics, we extended a many-particle theory for intersubband transitions including light propagation effects and carrier-carrier and carrier-phonon scattering to the nonlinear optical regime.[10,11,25] The additional equations needed for the nonlinear case are given in the Appendix.

Transmitted electric field transients calculated for different amplitudes of the input fields are presented in Figs. 4(d)–4(f) for sample H. The calculation reproduces both the shape and the temporal shift of the transmitted field with respect to the input fields. The calculated nonlinear transmission is shown in Fig. 5(a) (solid lines). It agrees well with the experiment apart from the low transmission in the linear case. The latter discrepancy is due to the approximation of carrier-carrier scattering in relaxation-rate approximation (see the Appendix), which clearly overestimates the linear absorption. The delay of the transmitted pulse is also reproduced well by the calculations [Fig. 5(b)].

The theory also yields the transient populations of the $n=2$ subband for each QW (Fig. 6). For sample L [Figs. 6(d)–6(f)] the populations for all QWs are nearly equal for all incident field amplitudes, since the reemitted fields by individual QWs are always much smaller than the incident fields. Thus the spatial amplitudes of the local fields and accordingly the populations follow the standing wave pattern due to the total reflection at the prism base, showing a maximum for the center QWs. For high enough incident field amplitudes [Figs. 6(e) and 6(f)] one observes coherent Rabi oscillations, i.e., a periodic variation of the $n=2$ population.

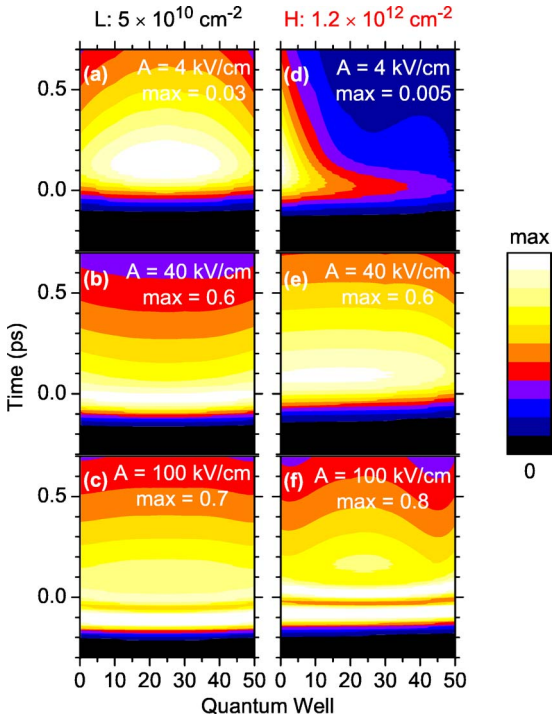

FIG. 6. (Color online) Calculated transient populations in the $n=2$ subbands of the different QWs in sample H [(a)–(c)] and in sample L [(d)–(f)] for different amplitudes A of the incident field. Note the different max values in the color encodings of the different contour plots. QW number 0 is the one hit first by the incident field [Fig. 2(a)].

While the populations in sample H are quite similar to the ones in sample L for high amplitudes [Figs. 6(b) and 6(c)], for low amplitudes [Fig. 6(a)] radiative coupling results in a completely different pattern. The population reaches high values only in the first few QWs. This is caused by the strong reemitted fields, which lead to progressively weaker local fields and concomitantly low populations. Because of the limit to the reemitted field amplitudes, for increasing incident amplitudes the local fields approach the incident fields.

VII. CONCLUSION

In conclusion, we have shown that radiative coupling has a strong influence on the linear and nonlinear optical properties of intersubband transitions. By changing the electron density and thus the strength of the radiative coupling in a multiple quantum well sample the change of transmission with increasing amplitude was found to be fundamentally different, transmission increase (bleaching) for low electron density, transmission decrease (induced absorption) for high density. Our results are relevant for all systems with a strong coupling to radiation fields, among them applications like the quantum cascade laser and other optoelectronic quantum devices.

ACKNOWLEDGMENTS

We gratefully acknowledge financial support by the Deutsche Forschungsgemeinschaft. One of the authors (I.W.)

is additionally supported by the "Berliner Programm zur Förderung von Frauen in Forschung und Lehre."

APPENDIX: EQUATIONS FOR THE POPULATIONS

To describe the experiments on a microscopic basis, Maxwell-Bloch equations for IS transitions,[9–11] including classical electromagnetic fields, Hartree-Fock and scattering effects on the second order Born level, have been solved. They consist of a set of polarization equations, which drive the optical field via Maxwell's equations, and population equations for the description of the nonlinear optical regime. The detailed equations for the polarizations are already given in Ref. 11. Using the same definitions, here we give the corresponding equations for the population:

$$\frac{d}{dt}f_{\mathbf{k}}^{1} = \Xi_{cf} + \Xi_{\text{exciton}} + \Xi_{\text{depol}} - \frac{\pi}{\hbar}f_{\mathbf{k}}^{1}\Gamma_{d}^{1,\text{out}} + \frac{\pi}{\hbar}(1-f_{\mathbf{k}}^{1})\Gamma_{d}^{1,\text{in}} + \sum_{\mathbf{Q}}\Gamma_{nl}^{1,cp} + \sum_{\mathbf{k}',\mathbf{q}}\Gamma_{nl}^{1,cc}, \tag{A1}$$

where Ξ_{cf} stems from the interaction of the carriers with the electric field. Ξ_{exciton} is the excitonic contribution and Ξ_{depol} the depolarization effect. $\Gamma_{d}^{i,\text{in}}$ denotes the diagonal in-scattering and $\Gamma_{d}^{i,\text{out}}$ the corresponding diagonal out-scattering rate. The total rate, which is used in Ref. 11, is the sum of in- and out-scattering rates, $\Gamma_{d}^{i}=\Gamma_{d}^{i,\text{in}}+\Gamma_{d}^{i,\text{out}}$. $\Gamma_{nl}^{i,cp}$ is the contribution nonlinear in the polarization from the carrier-phonon interaction and $\Gamma_{nl}^{i,cc}$ the nonlinear contribution from carrier-carrier scattering. In the following we will give the detailed expressions for these contributions.

The carrier-field interaction is given by

$$\Xi_{cf} = \frac{i}{\hbar}d_{21}E_{z}(t)(p_{\mathbf{k}}^{12}-p_{\mathbf{k}}^{21}) \tag{A2}$$

d_{21} is the electric dipole transition matrix element for the intersubband transition and $E_{z}(t)$ the local field in the quantum well. This local field is equal to the sum of the incident field and of the fields emitted from all quantum wells, which depend on the intersubband polarizations (see Appendix A in Ref. 11).

The excitonic and depolarization contributions are

$$\Xi_{\text{exciton}} = \frac{i}{\hbar}\sum_{\mathbf{q}}(V_{\mathbf{q}}^{1212}p_{\mathbf{k}-\mathbf{q}}^{21}+V_{\mathbf{q}}^{2112}p_{\mathbf{k}-\mathbf{q}}^{12})p_{\mathbf{k}}^{12} + \text{c.c.}, \tag{A3}$$

$$\Xi_{\text{depol}} = -\frac{i}{\hbar}V_{0}^{2112}\sum_{\mathbf{k}'}(p_{\mathbf{k}'}^{12}+p_{\mathbf{k}'}^{21})p_{\mathbf{k}}^{12} + \text{c.c.} \tag{A4}$$

The in- and out-scattering rates are given by

$$\begin{aligned}\Gamma_{d}^{1,\text{in}} = \sum_{\mathbf{Q}} f_{\mathbf{k}+\mathbf{Q}_{\parallel}}^{1}[&|g_{\mathbf{Q}}^{11}|^{2}\{\delta(-\epsilon_{\mathbf{k}}^{1}+\epsilon_{\mathbf{k}+\mathbf{Q}_{\parallel}}^{1}-\hbar\omega_{\text{LO}})(n_{\mathbf{Q}}+1)+\delta(-\epsilon_{\mathbf{k}}^{1}+\epsilon_{\mathbf{k}+\mathbf{Q}_{\parallel}}^{1}+\hbar\omega_{\text{LO}})n_{\mathbf{Q}}\}\\ &+|g_{\mathbf{Q}}^{12}|^{2}\{\delta(-\epsilon_{\mathbf{k}}^{2}+\epsilon_{\mathbf{k}+\mathbf{Q}_{\parallel}}^{1}-\hbar\omega_{\text{LO}})(n_{\mathbf{Q}}+1)+\delta(-\epsilon_{\mathbf{k}}^{2}+\epsilon_{\mathbf{k}+\mathbf{Q}_{\parallel}}^{1}+\hbar\omega_{\text{LO}})n_{\mathbf{Q}}\}]\\ &+\sum_{\mathbf{k}',\mathbf{q}}[\delta(\epsilon_{\mathbf{k}}^{1}+\epsilon_{\mathbf{k}'}^{1}-\epsilon_{\mathbf{k}'-\mathbf{q}}^{1}-\epsilon_{\mathbf{k}+\mathbf{q}}^{1})V_{\mathbf{q}}^{1111}(2V_{\mathbf{q}}^{1111}-V_{\mathbf{k}'-\mathbf{k}-\mathbf{q}}^{1111})\{f_{\mathbf{k}'-\mathbf{q}}^{1}f_{\mathbf{k}+\mathbf{q}}^{1}(1-f_{\mathbf{k}'}^{1})\}\\ &+\delta(\epsilon_{\mathbf{k}}^{1}+\epsilon_{\mathbf{k}'}^{1}-\epsilon_{\mathbf{k}'-\mathbf{q}}^{2}-\epsilon_{\mathbf{k}+\mathbf{q}}^{2})V_{\mathbf{q}}^{1122}(2V_{\mathbf{q}}^{1122}-V_{\mathbf{k}'-\mathbf{k}-\mathbf{q}}^{1122})\{f_{\mathbf{k}'-\mathbf{q}}^{2}f_{\mathbf{k}+\mathbf{q}}^{2}(1-f_{\mathbf{k}'}^{1})\}\\ &+\delta(\epsilon_{\mathbf{k}}^{1}+\epsilon_{\mathbf{k}'}^{2}-\epsilon_{\mathbf{k}'-\mathbf{q}}^{1}-\epsilon_{\mathbf{k}+\mathbf{q}}^{2})V_{\mathbf{q}}^{1221}(2V_{\mathbf{q}}^{1221}-V_{\mathbf{k}'-\mathbf{k}-\mathbf{q}}^{1212})\{f_{\mathbf{k}'-\mathbf{q}}^{1}f_{\mathbf{k}+\mathbf{q}}^{2}(1-f_{\mathbf{k}'}^{2})\}\\ &+\delta(\epsilon_{\mathbf{k}}^{1}+\epsilon_{\mathbf{k}'}^{2}-\epsilon_{\mathbf{k}'-\mathbf{q}}^{2}-\epsilon_{\mathbf{k}+\mathbf{q}}^{1})V_{\mathbf{q}}^{1212}(2V_{\mathbf{q}}^{1212}-V_{\mathbf{k}'-\mathbf{k}-\mathbf{q}}^{1221})\{f_{\mathbf{k}'-\mathbf{q}}^{2}f_{\mathbf{k}+\mathbf{q}}^{2}(1-f_{\mathbf{k}'}^{1})\}],\end{aligned} \tag{A5}$$

$$\begin{aligned}\Gamma_{d}^{1,\text{out}} = \sum_{\mathbf{Q}} (1-f_{\mathbf{k}+\mathbf{Q}_{\parallel}}^{1})[&|g_{\mathbf{Q}}^{11}|^{2}\{\delta(-\epsilon_{\mathbf{k}}^{1}+\epsilon_{\mathbf{k}+\mathbf{Q}_{\parallel}}^{1}+\hbar\omega_{\text{LO}})(n_{\mathbf{Q}}+1)+\delta(-\epsilon_{\mathbf{k}}^{1}+\epsilon_{\mathbf{k}+\mathbf{Q}_{\parallel}}^{1}-\hbar\omega_{\text{LO}})n_{\mathbf{Q}}\}\\ &+|g_{\mathbf{Q}}^{12}|^{2}\{\delta(-\epsilon_{\mathbf{k}}^{2}+\epsilon_{\mathbf{k}+\mathbf{Q}_{\parallel}}^{1}+\hbar\omega_{\text{LO}})(n_{\mathbf{Q}}+1)+\delta(-\epsilon_{\mathbf{k}}^{2}+\epsilon_{\mathbf{k}+\mathbf{Q}_{\parallel}}^{1}-\hbar\omega_{\text{LO}})n_{\mathbf{Q}}\}]\\ &+\sum_{\mathbf{k}',\mathbf{q}}[\delta(\epsilon_{\mathbf{k}}^{1}+\epsilon_{\mathbf{k}'}^{1}-\epsilon_{\mathbf{k}'-\mathbf{q}}^{1}-\epsilon_{\mathbf{k}+\mathbf{q}}^{1})V_{\mathbf{q}}^{1111}(2V_{\mathbf{q}}^{1111}-V_{\mathbf{k}'-\mathbf{k}-\mathbf{q}}^{1111})\{f_{\mathbf{k}'}^{1}(1-f_{\mathbf{k}'-\mathbf{q}}^{1})(1-f_{\mathbf{k}+\mathbf{q}}^{1})\}\\ &+\delta(\epsilon_{\mathbf{k}}^{1}+\epsilon_{\mathbf{k}'}^{1}-\epsilon_{\mathbf{k}'-\mathbf{q}}^{2}-\epsilon_{\mathbf{k}+\mathbf{q}}^{2})V_{\mathbf{q}}^{1122}(2V_{\mathbf{q}}^{1122}-V_{\mathbf{k}'-\mathbf{k}-\mathbf{q}}^{1122})\{f_{\mathbf{k}'}^{1}(1-f_{\mathbf{k}'-\mathbf{q}}^{2})(1-f_{\mathbf{k}+\mathbf{q}}^{2})\}\\ &+\delta(\epsilon_{\mathbf{k}}^{1}+\epsilon_{\mathbf{k}'}^{2}-\epsilon_{\mathbf{k}'-\mathbf{q}}^{1}-\epsilon_{\mathbf{k}+\mathbf{q}}^{2})V_{\mathbf{q}}^{1221}(2V_{\mathbf{q}}^{1221}-V_{\mathbf{k}'-\mathbf{k}-\mathbf{q}}^{1212})\{f_{\mathbf{k}'}^{2}(1-f_{\mathbf{k}'-\mathbf{q}}^{1})(1-f_{\mathbf{k}+\mathbf{q}}^{2})\}\\ &+\delta(\epsilon_{\mathbf{k}}^{1}+\epsilon_{\mathbf{k}'}^{2}-\epsilon_{\mathbf{k}'-\mathbf{q}}^{2}-\epsilon_{\mathbf{k}+\mathbf{q}}^{1})V_{\mathbf{q}}^{1212}(2V_{\mathbf{q}}^{1212}-V_{\mathbf{k}'-\mathbf{k}-\mathbf{q}}^{1221})\{f_{\mathbf{k}'}^{2}(1-f_{\mathbf{k}'-\mathbf{q}}^{2})(1-f_{\mathbf{k}+\mathbf{q}}^{1})\}].\end{aligned} \tag{A6}$$

In both expressions the first sum comes from the carrier-phonon, the second from the carrier-carrier interaction.

The terms nonlinear in the polarization contain products of the form $p_{\mathbf{k}}^{ij}p_{\mathbf{k}'}^{i'j'}$. They are given by

$$\Gamma_{nl}^{1,cp} = -\delta(-\epsilon_{\mathbf{k}}^{2}+\epsilon_{\mathbf{k}+\mathbf{Q}_{\parallel}}^{2}-\hbar\omega_{\mathrm{LO}})g_{\mathbf{Q}}^{11}g_{\mathbf{Q}}^{22*}p_{\mathbf{k}}^{21}p_{\mathbf{k}+\mathbf{Q}_{\parallel}}^{12}+\delta(-\epsilon_{\mathbf{k}}^{2}+\epsilon_{\mathbf{k}+\mathbf{Q}_{\parallel}}^{2}+\hbar\omega_{\mathrm{LO}})g_{\mathbf{Q}}^{22*}g_{\mathbf{Q}}^{11}p_{\mathbf{k}}^{12}p_{\mathbf{k}+\mathbf{Q}_{\parallel}}^{21}$$
$$-\delta(-\epsilon_{\mathbf{k}}^{2}+\epsilon_{\mathbf{k}+\mathbf{Q}_{\parallel}}^{1}-\hbar\omega_{\mathrm{LO}})g_{\mathbf{Q}}^{21}g_{\mathbf{Q}}^{12*}p_{\mathbf{k}}^{21}p_{\mathbf{k}+\mathbf{Q}_{\parallel}}^{21}+\delta(-\epsilon_{\mathbf{k}}^{2}+\epsilon_{\mathbf{k}+\mathbf{Q}_{\parallel}}^{1}+\hbar\omega_{\mathrm{LO}})g_{\mathbf{Q}}^{21*}g_{\mathbf{Q}}^{12}p_{\mathbf{k}}^{12}p_{\mathbf{k}+\mathbf{Q}_{\parallel}}^{12}+\mathrm{c.c.}, \tag{A7}$$

$$\Gamma_{nl}^{1,cc} = \delta(\epsilon_{\mathbf{k}}^{1}+\epsilon_{\mathbf{k}'}^{1}-\epsilon_{\mathbf{k}'-\mathbf{q}}^{1}-\epsilon_{\mathbf{k}+\mathbf{q}}^{1})(2V_{\mathbf{q}}^{1111}-V_{\mathbf{k}'-\mathbf{k}-\mathbf{q}}^{1111})[V_{\mathbf{q}}^{1221}(1-f_{\mathbf{k}}^{1}-f_{\mathbf{k}'}^{1})p_{\mathbf{k}+\mathbf{q}}^{21}p_{\mathbf{k}'-\mathbf{q}}^{21}+V_{\mathbf{q}}^{1221}(f_{\mathbf{k}}^{1}-f_{\mathbf{k}'-\mathbf{q}}^{1})p_{\mathbf{k}+\mathbf{q}}^{12}p_{\mathbf{k}'}^{21}$$
$$+V_{\mathbf{q}}^{1212}(f_{\mathbf{k}}^{1}-f_{\mathbf{k}+\mathbf{q}}^{1})p_{\mathbf{k}'}^{12}p_{\mathbf{k}'-\mathbf{q}}^{21}]+\delta(\epsilon_{\mathbf{k}}^{1}+\epsilon_{\mathbf{k}'}^{1}-\epsilon_{\mathbf{k}'-\mathbf{q}}^{2}-\epsilon_{\mathbf{k}+\mathbf{q}}^{2})(2V_{\mathbf{q}}^{1221}-V_{\mathbf{k}'-\mathbf{k}-\mathbf{q}}^{1221})[V_{\mathbf{q}}^{1111}(1-f_{\mathbf{k}}^{1}-f_{\mathbf{k}'}^{1})p_{\mathbf{k}+\mathbf{q}}^{21}p_{\mathbf{k}'-\mathbf{q}}^{21}$$
$$+V_{\mathbf{q}}^{1221}(f_{\mathbf{k}}^{1}-f_{\mathbf{k}+\mathbf{q}}^{2})p_{\mathbf{k}'-\mathbf{q}}^{21}p_{\mathbf{k}}^{21}+V_{\mathbf{q}}^{1212}(f_{\mathbf{k}}^{1}-f_{\mathbf{k}'-\mathbf{q}}^{2})p_{\mathbf{k}'}^{21}p_{\mathbf{k}+\mathbf{q}}^{21}]+\delta(\epsilon_{\mathbf{k}}^{1}+\epsilon_{\mathbf{k}'}^{2}-\epsilon_{\mathbf{k}'-\mathbf{q}}^{1}-\epsilon_{\mathbf{k}+\mathbf{q}}^{2})(2V_{\mathbf{q}}^{1221}-V_{\mathbf{k}'-\mathbf{k}-\mathbf{q}}^{1212})$$
$$\times[V_{\mathbf{q}}^{1111}(f_{\mathbf{k}}^{1}-f_{\mathbf{k}'-\mathbf{q}}^{1})p_{\mathbf{k}+\mathbf{q}}^{12}p_{\mathbf{k}'}^{21}+V_{\mathbf{q}}^{1221}(f_{\mathbf{k}}^{1}-f_{\mathbf{k}+\mathbf{q}}^{2})p_{\mathbf{k}'-\mathbf{q}}^{21}p_{\mathbf{k}'}^{21}+V_{\mathbf{q}}^{1212}(1-f_{\mathbf{k}}^{1}-f_{\mathbf{k}'}^{2})p_{\mathbf{k}'-\mathbf{q}}^{21}p_{\mathbf{k}+\mathbf{q}}^{12}]$$
$$+\delta(\epsilon_{\mathbf{k}}^{1}+\epsilon_{\mathbf{k}'}^{2}-\epsilon_{\mathbf{k}'-\mathbf{q}}^{2}-\epsilon_{\mathbf{k}+\mathbf{q}}^{1})(2V_{\mathbf{q}}^{1212}-V_{\mathbf{k}'-\mathbf{k}-\mathbf{q}}^{1221})[V_{\mathbf{q}}^{1111}(f_{\mathbf{k}}^{1}-f_{\mathbf{k}+\mathbf{q}}^{1})p_{\mathbf{k}'}^{12}p_{\mathbf{k}'-\mathbf{q}}^{21}+V_{\mathbf{q}}^{1221}(f_{\mathbf{k}}^{1}-f_{\mathbf{k}'-\mathbf{q}}^{2})p_{\mathbf{k}+\mathbf{q}}^{21}p_{\mathbf{k}'}^{21}$$
$$+V_{\mathbf{q}}^{1221}(1-f_{\mathbf{k}}^{1}-f_{\mathbf{k}'}^{2})p_{\mathbf{k}'-\mathbf{q}}^{21}p_{\mathbf{k}+\mathbf{q}}^{12}]+\delta(\epsilon_{\mathbf{k}}^{2}+\epsilon_{\mathbf{k}'}^{2}-\epsilon_{\mathbf{k}'-\mathbf{q}}^{2}-\epsilon_{\mathbf{k}+\mathbf{q}}^{2})(2V_{\mathbf{q}}^{2222}-V_{\mathbf{k}'-\mathbf{k}-\mathbf{q}}^{2222})[V_{\mathbf{q}}^{1212}(f_{\mathbf{k}'}^{2}-f_{\mathbf{k}'-\mathbf{q}}^{2})p_{\mathbf{k}}^{12}p_{\mathbf{k}+\mathbf{q}}^{21}$$
$$+V_{\mathbf{q}}^{1221}(f_{\mathbf{k}'}^{2}-f_{\mathbf{k}+\mathbf{q}}^{2})p_{\mathbf{k}'-\mathbf{q}}^{21}p_{\mathbf{k}}^{12}-V_{\mathbf{q}}^{1221}(1-f_{\mathbf{k}+\mathbf{q}}^{2}-f_{\mathbf{k}'-\mathbf{q}}^{2})p_{\mathbf{k}'}^{21}p_{\mathbf{k}}^{21}]+\delta(\epsilon_{\mathbf{k}}^{2}+\epsilon_{\mathbf{k}'}^{2}-\epsilon_{\mathbf{k}'-\mathbf{q}}^{1}-\epsilon_{\mathbf{k}+\mathbf{q}}^{1})(2V_{\mathbf{q}}^{1221}-V_{\mathbf{k}'-\mathbf{k}-\mathbf{q}}^{1221})$$
$$\times[V_{\mathbf{q}}^{1212}(f_{\mathbf{k}'}^{2}-f_{\mathbf{k}+\mathbf{q}}^{1})p_{\mathbf{k}}^{12}p_{\mathbf{k}'-\mathbf{q}}^{12}+V_{\mathbf{q}}^{1221}(f_{\mathbf{k}'}^{2}-f_{\mathbf{k}'-\mathbf{q}}^{1})p_{\mathbf{k}}^{21}p_{\mathbf{k}+\mathbf{q}}^{21}-V_{\mathbf{q}}^{1111}(1-f_{\mathbf{k}+\mathbf{q}}^{1}-f_{\mathbf{k}'-\mathbf{q}}^{1})p_{\mathbf{k}}^{21}p_{\mathbf{k}'}^{21}]$$
$$+\delta(\epsilon_{\mathbf{k}}^{2}+\epsilon_{\mathbf{k}'}^{1}-\epsilon_{\mathbf{k}'-\mathbf{q}}^{2}-\epsilon_{\mathbf{k}+\mathbf{q}}^{1})(2V_{\mathbf{q}}^{1221}-V_{\mathbf{k}'-\mathbf{k}-\mathbf{q}}^{1212})[V_{\mathbf{q}}^{1221}(f_{\mathbf{k}'}^{1}-f_{\mathbf{k}'-\mathbf{q}}^{2})p_{\mathbf{k}}^{21}p_{\mathbf{k}+\mathbf{q}}^{21}+V_{\mathbf{q}}^{1111}(f_{\mathbf{k}'}^{1}-f_{\mathbf{k}+\mathbf{q}}^{1})p_{\mathbf{k}}^{12}p_{\mathbf{k}'-\mathbf{q}}^{21}$$
$$-V_{\mathbf{q}}^{1212}(1-f_{\mathbf{k}'-\mathbf{q}}^{2}-f_{\mathbf{k}+\mathbf{q}}^{1})p_{\mathbf{k}}^{12}p_{\mathbf{k}'}^{21}]+\delta(\epsilon_{\mathbf{k}}^{2}+\epsilon_{\mathbf{k}'}^{1}-\epsilon_{\mathbf{k}'-\mathbf{q}}^{1}-\epsilon_{\mathbf{k}+\mathbf{q}}^{2})(2V_{\mathbf{q}}^{1212}-V_{\mathbf{k}'-\mathbf{k}-\mathbf{q}}^{1221})$$
$$\times[V_{\mathbf{q}}^{1221}(f_{\mathbf{k}'}^{1}-f_{\mathbf{k}+\mathbf{q}}^{2})p_{\mathbf{k}}^{12}p_{\mathbf{k}'-\mathbf{q}}^{12}+V_{\mathbf{q}}^{1111}(f_{\mathbf{k}'}^{1}-f_{\mathbf{k}'-\mathbf{q}}^{1})p_{\mathbf{k}}^{12}p_{\mathbf{k}+\mathbf{q}}^{21}-V_{\mathbf{q}}^{1221}(1-f_{\mathbf{k}'-\mathbf{q}}^{1}-f_{\mathbf{k}+\mathbf{q}}^{2})p_{\mathbf{k}}^{12}p_{\mathbf{k}'}^{21}]+\mathrm{c.c.} \tag{A8}$$

Unfortunately, for the calculation of the nonlinear response of a radiatively coupled multiple quantum well system it is not possible to use the full equations for the carrier-carrier scattering given above, because they cannot be solved within a reasonable computing time. Instead we use for the carrier-carrier scattering the relaxation rate approximation, which includes the following: (i) the nondiagonal terms are neglected, (ii) the diagonal terms are approximated by the scattering rate at $k=0$. This scattering rate is updated after every time step using a Fermi-Dirac distribution, the parameters (chemical potential and carrier temperature) of which are determined so that the number of carriers and the energy are equal to the actual distribution. In this way the theory includes excitation induced dephasing processes,[26] which were shown experimentally to be important for high electron densities.[24]

Neglecting the nondiagonal terms in carrier-carrier scattering tends to somewhat overestimate its effect on the dephasing. In the linear case this leads for sample *H* to broader absorption lines than using the full theory.[11] Another effect is that the absorption for low amplitudes is calculated too high [see Fig. 5(a)].

*Present address: Harvard University, Cambridge, MA 02138, USA.
†Electronic address: reimann@mbi-berlin.de
‡Electronic address: woerner@mbi-berlin.de
§Present address: Sandia National Laboratories, Albuquerque, NM 87185, USA.

[1] J. Shah, *Ultrafast Spectroscopy of Semiconductors and Semiconductor Nanostructures*, 2nd ed. (Springer, Berlin, 1999).
[2] M. Hübner, J. Kuhl, T. Stroucken, A. Knorr, S. W. Koch, R. Hey, and K. Ploog, Phys. Rev. Lett. **76**, 4199 (1996).
[3] S. Haas, T. Stroucken, M. H. J. Kuhl, B. Grote, A. Knorr, F. Jahnke, S. W. Koch, R. Hey, and K. Ploog, Phys. Rev. B **57**, 14860 (1998).
[4] J. P. Prineas, J. Y. Zhou, J. Kuhl, H. M. Gibbs, G. Khitrova, S. W. Koch, and A. Knorr, Appl. Phys. Lett. **81**, 4332 (2002).
[5] N. C. Nielsen, J. Kuhl, M. Schaarschmidt, J. Förstner, A. Knorr, S. W. Koch, H. M. Gibbs, G. Khitrova, and H. Giessen, Phys. Status Solidi C **0**, 1484 (2003).
[6] T. Elsaesser and M. Woerner, Phys. Rep. **321**, 253 (1999).
[7] A. Liu, Phys. Rev. B **55**, 7796 (1997).
[8] M. Zaluzny and C. Nalewajko, Phys. Rev. B **59**, 13043 (1999).
[9] J. Förstner, K. J. Ahn, J. Danckwerts, M. Schaarschmidt, I. Waldmüller, C. Weber, and A. Knorr, Phys. Status Solidi B **234**, 155 (2002).
[10] I. Waldmüller, M. Woerner, J. Förstner, and A. Knorr, Phys. Status Solidi B **238**, 474 (2003).
[11] I. Waldmüller, J. Förstner, S. C. Lee, A. Knorr, M. Woerner, K. Reimann, R. A. Kaindl, T. Elsaesser, R. Hey, and K. H. Ploog, Phys. Rev. B **69**, 205307 (2004).
[12] D. Dini, R. Köhler, A. Tredicucci, G. Biasiol, and L. Sorba, Phys. Rev. Lett. **90**, 116401 (2003).
[13] C. W. Luo, K. Reimann, M. Woerner, T. Elsaesser, R. Hey, and K. H. Ploog, Phys. Rev. Lett. **92**, 047402 (2004).
[14] F. Eickemeyer, M. Woerner, A. M. Weiner, T. Elsaesser, R. Hey, and K. H. Ploog, Appl. Phys. Lett. **79**, 165 (2001).
[15] The small reflections at the side facets and the time delay are taken care of by measuring E_{in} after having passed through an undoped sample of identical shape.

[16] T. Stroucken, A. Knorr, P. Thomas, and S. W. Koch, Phys. Rev. B **53**, 2026 (1996).

[17] Plane waves are an adequate approximation for our problem since the experimental beam diameter within the QW plane ($\approx$200 μm) is much larger than the length of the interaction region perpendicular to the wells (3 μm).

[18] The IS absorption cross section σ_{IS} is inversely proportional to the linewidth of the IS transition. Since for sample L the IS linewidth increases with T_L (for sample H the linewidth is nearly independent of T_L), different T_L lead to different σ_{IS} and thus to different ξ, resulting in the five experimental points shown for sample L. Another consequence of this dependence on the linewidth is that the value of ξ for the $1 \leftrightarrow 2$ transition in sample H is slightly lower than expected from the 24-times higher n_s.

[19] In our samples, the distance between the first and the last QW is 1.5 μm. This is not completely negligible compared to the IS transition wavelength of 12 μm, which is one reason that the experimental data do not agree perfectly with the simple model. The microscopic theory developed in this paper, however, accounts fully for the real geometry of our samples.

[20] J. E. Sipe, J. Opt. Soc. Am. B **4**, 481 (1987).

[21] K. Reimann, R. P. Smith, A. M. Weiner, T. Elsaesser, and M. Woerner, Opt. Lett. **28**, 471 (2003).

[22] Q. Wu and X.-C. Zhang, Appl. Phys. Lett. **71**, 1285 (1997).

[23] Here we show the transmitted light $E_{\mathrm{out}}(t)$ and not the reemitted light $E_{\mathrm{em}}(t)=E_{\mathrm{out}}(t)-E_{\mathrm{in}}(t)$ as in Ref. 13.

[24] R. A. Kaindl, K. Reimann, M. Woerner, T. Elsaesser, R. Hey, and K. H. Ploog, Phys. Rev. B **63**, 161308(R) (2001).

[25] J. Li and C. Z. Ning, Phys. Rev. B **70**, 125309 (2004).

[26] F. Jahnke, M. Kira, and S. W. Koch, Z. Phys. B: Condens. Matter **104**, 559 (1997).